Original Paper

Cavitation Surge in a Small Model Test Facility Simulating a Hydraulic Power Plant

Koichi Yonezawa[1], Daisuke Konishi[1], Kazuyoshi Miyagawa[2]
François Avellan[3], Peter Doerfler[4], and Yoshinobu Tsujimoto[1]

[1]Graduate School of Engineering Science, Osaka University
1-3, Machikaneyama-cho, Toyonaka, Osaka 560-8531, Japan
yonezawa@me.es.osaka-u.ac.jp, tujimoto@me.es.osaka-u.ac.jp
[2]Faculty of Science and Engineering, Waseda University
3-4-1, Ohkubo, Shinjuku-ku, Tokyo, 169-8555, Japan, k-miyagawa@waseda.jp
[3] Laboratory for Hydraulic Machines, École Polytechnique Fédérale de Lausanne
Avenue de Cour 33bis, Lausanne, CH-1007, Switzerland, francois.avellan@epfl.ch
[4]R&D Department, Andritz Hydro Ltd.
Postfach 2602, 8021 Zurich, Switzerland, peter.doerfler@andritz.com

Abstract

Model tests and CFD were carried out to find out the cause of cavitation surge in hydraulic power plants. In experiments the cavitation surge was observed at flow rates higher and lower than the swirl free flow rate, both with and without a surge tank placed just upstream of the inlet volute. The surge frequency at smaller flow rate was much smaller than the swirl mode frequency caused by the whirl of vortex rope. An unsteady CFD was carried out with two boundary conditions: (1) the flow rate is fixed to be constant at the volute inlet, (2) the total pressure is kept constant at the volute inlet, corresponding to the experiments without/with the surge tank. The surge was observed with both boundary conditions at both higher and lower flow rates. Discussions as to the cause of the surge are made based on additional tests with an orifice at the diffuser exit, and with the diffuser replaced with a straight pipe.

Keywords: Draft tube surge, cavitation, hydro turbine

1. Introduction

Cavitation surge sometimes occurs at higher flow rate than the swirl free flow rate and this is known as overload surge. By using a one-dimensional model [1,2] it was found the pressure recovery in the draft tube, and the swirl flow at the runner discharge can be the causes of cavitation surge in hydropower system. If the flow through the draft tube increases, the pressure at the runner exit will decrease due to the increase of the pressure recovery. Then the cavity volume will increase and causes further increase of the draft tube flow. This effect occurs at any flow rate. It has been shown by tests using a conical diffuser without a runner that the diffuser effects can be a cause of the surge [3], [4]. If the flow through the runner increases at part load/overload, the swirl at runner exit will decrease/increase. Then the cavity volume at the core of the swirl flow will decrease/increase due to the decrease/increase of the pressure decrease caused by the centrifugal force on the swirl flow and the runner flow will increase/decrease. So the swirl flow effects destabilize the flow at part load but stabilize at overload. Combining these effects, the flow is always destabilized at part load, if we neglect the delay of cavity response.   However, the instability at part load is extremely rare in real plants. So, we need to fill up the gap between the 1-D theory and the reality. It has been considered that the flow oscillation at part load is a forced oscillation caused by the whirl of corkscrew vortex structure and the surge mode oscillation becomes significant if the vortex whirl frequency agrees with the resonant frequency of the system [5,6]. The present study was intended to determine the effects of the swirl flow from the runner on the cavitation instabilities, especially at part load.
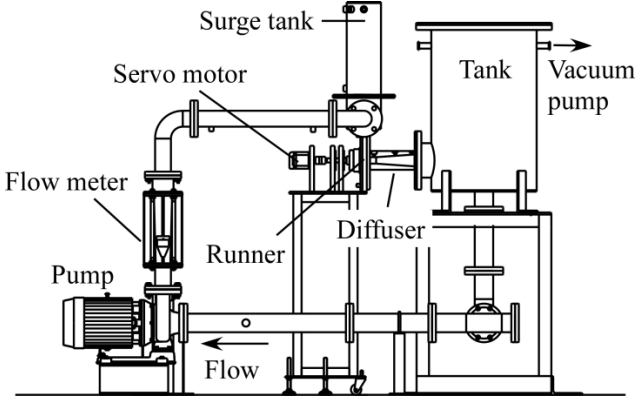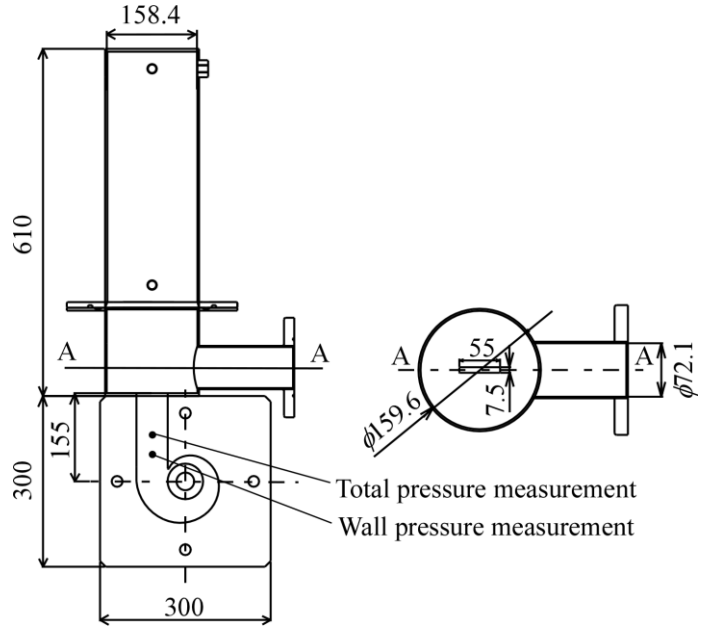
Fig. 1 Experimental facility

(a) Side view (b) Top view

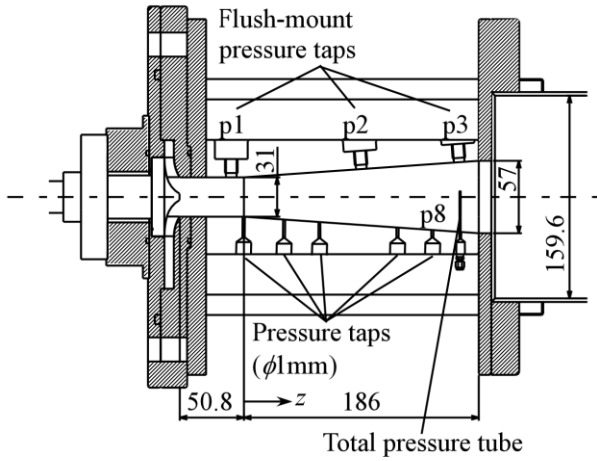**Fig. 2** Details around surge tank and inlet volute
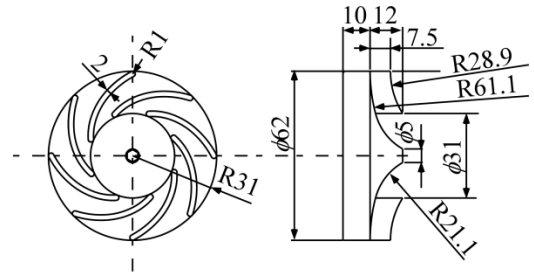

Fig. 3 Conical diffuser

Fig. 4 Runner geometry

2. Experimental Set Up and CFD

Figure 1 shows the experimental facility. The cavitation number was adjusted by adjusting the pressure in the tank downstream of the diffuser. Tests were carried out with and without the surge tank (see Fig.2) placed just upstream of the inlet volute, to examine the effect of the components upstream of the volute. Some amount of air is put in both tanks to keep the pressure there to be nearlyconstant. Major tests were made with keeping the runner speed to be 3,000rpm. Pressure fluctuations p1, p2 and p3 near the inlet, middle and exit of the diffuser are used to monitor the oscillations (see Fig.3). Pressure is measured at two circumferential locations at each axial locations and the phase difference is used to identify the mode of oscillations.

Figure 4 shows the geometry of the runner with the inlet and outlet blade angles of 27.7deg and 24.9deg, respectively. It is open shroud type and the tip clearance is kept to be 0.2mm. It was designed so that the flow enters the runnuer without incidence and leaves the runner without swirl at the design flow rate of Q_d=150L/min at 3,000rpn The rotational speed of the runner was kept constant using a servo motor.

Figure 5 shows the velocity triangles at the inlet and outlet of the runner. Solid vectors are obtained by assuming that the flow is tangent to the volute and blade surface, and the broken vectors are the results of CFD at the center of the flow channel.

Figure 6 shows the head coefficient $\psi_R = \Delta p /(0.5\rho v^2)$ of the runner where $\Delta p = p_{inlet} - p1$ and v is the runner outlet periferal velocity. The inlet pressure p_{inlet} was evaluated at the wall pressure tap shown in Fig.2. Table 1 shows the swirl number

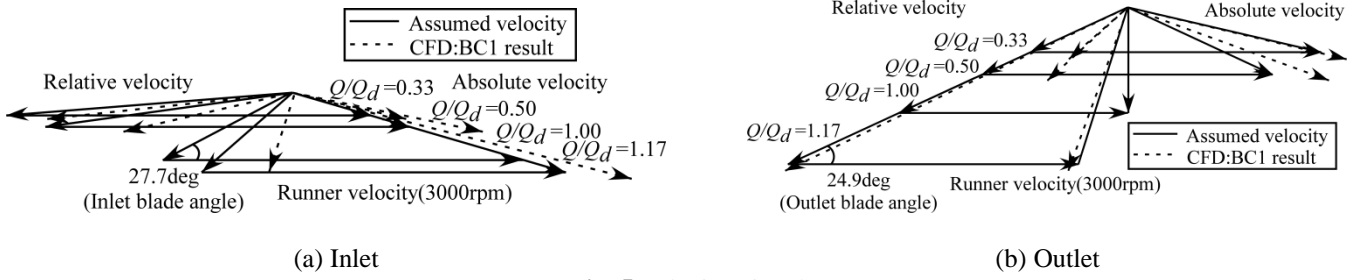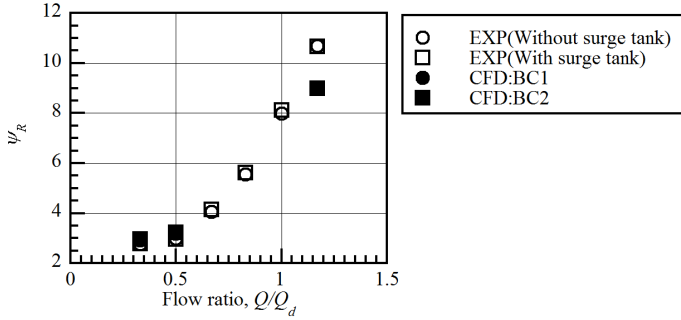$$m \equiv \int_0^{r_i} V_z r V_\theta r dr / r_i \int_0^{r_i} V_z^2 r dr \tag{1}$$

153

(a) Inlet   (b) Outlet

Fig. 5 Velocity triangle

Fig. 6 Head coefficient of the runner

Table 1 Swirl number

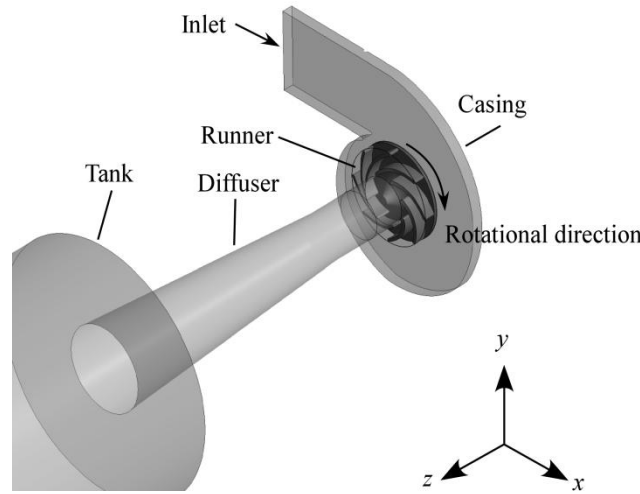| Q/Q_d	m_{nom}	m_{LDV}	$m_{CFD:BC1}$
0.33	3.33	2.11	1.65
0.50	1.66	1.17	1.31
1.17	-0.24	-0.45	-0.20

Fig. 7 Computational domain

where r_i is the runner exit/diffuser inlet radius, V_z and V_θ are the axial and circumferential flow velocities at the diffuser inlet. The swirl number based on LDV measurements (m_{LDV}) and CFD (m_{CFD}) are shown along with the nominal value (m_{nom}) obtained by assuming that the flow is uniform and along the runner blade surface.

Figure 7 shows the CFD domain for 3D unsteady cavitating flow analysis. The geometry is the same as experiments except that the discharge tank is replaced with a cylindrical one with the diameter of 3 times the diffuser exit diameter and the lenth of 2 times the diffuser length. The total grid number is 1,339,847 with 274,752 grids in the diffuser. ANSYS CFX13 has been used with the option of cavitation model based on simplified Rayleigh-Plesset equation and with SAS-SST turbulence model.

Two types of boundary conditions are examined: constant inlet normal velocity and constant outlet static pressure (BC1) and constant inlet total pressure and constant outlet static pressure (BC2) corresponding to the experiments without and with the surge tank at the volute inlet. The mesh size and the time step 1/100 of rotational period has been determined so that the continuity equation   is satisfied with acceptable level, were the cavity volume V_c is determined from the integration of the void fraction, Q_1 and Q_2 are the inlet and outlet flow rate.

3. Results and discussions

3.1 Pressure fluctuation mode and frequency

Figure 8 shows the static pressure distribution $\psi_s = (p - p_v)/(0.5\rho v^2)$ in the diffuser, where p_v is the vapor pressure and v the runner velocity at the outlet, at the cavitation number $\sigma = (p_t + \rho g h - p_v)/(0.5\rho v^2) = 0.84$, where p_t is the air pressure at the upper part of the discharge tank, h the water level above the center of the diffuser exit. If we neglect the dynamic pressure at the diffuser outlet, Thoma's cavitation number σ_T can be approximately evaluated from $\sigma_T = \sigma/\psi_R$ using the head coefficient ψ_R of the runner shown in Fig.6.
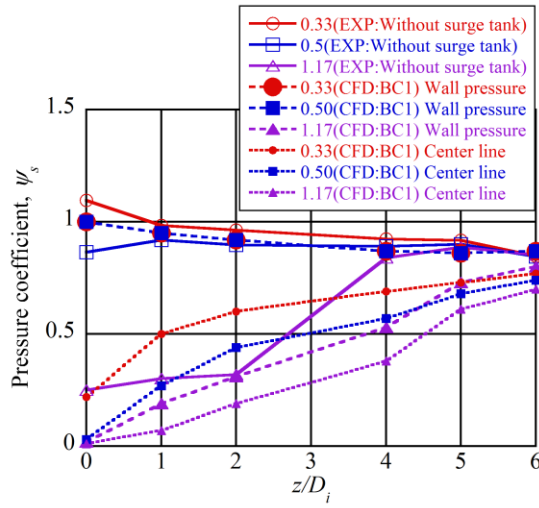
Fig. 8 Axial pressure distribution at σ=0.84

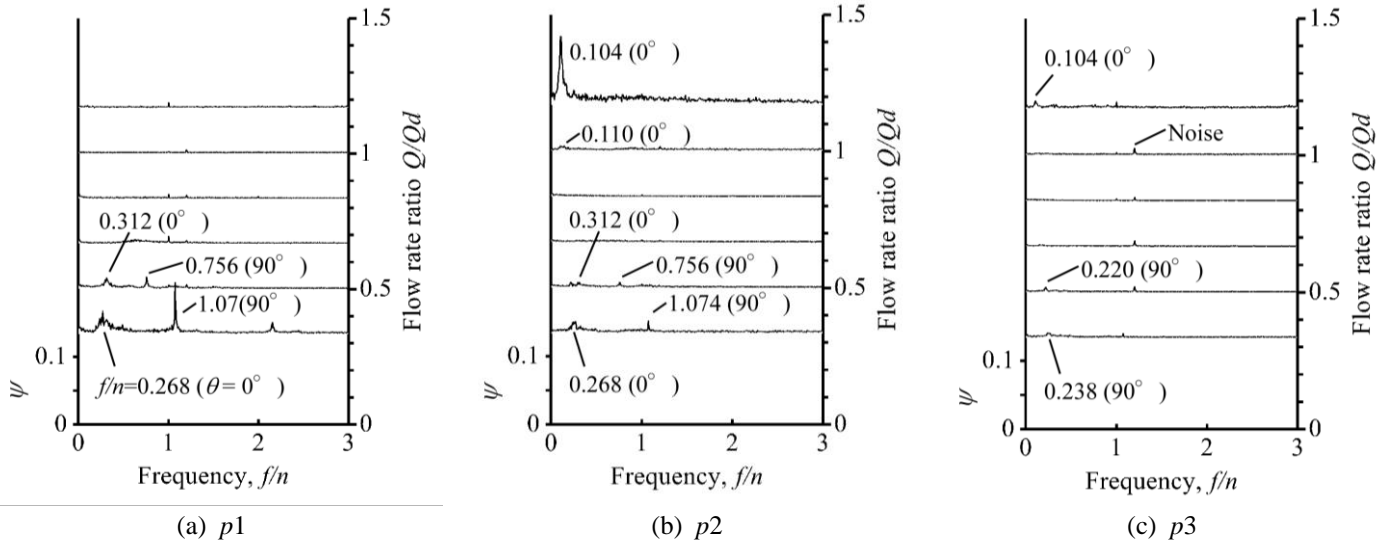(a) $p1$ (b) $p2$ (c) $p3$

Fig. 9 Spectra of pressure fluctuation, 3000rpm, with surge tank, $\sigma = 0.84$

The origin of the axial coordinate z/D_i=0 is placed at the position in the diffuser where the crosssectional area starts to increase. At Q/Q_d=0.50 and 0.33, the pressure distribution has negative slope on the casing wall. However, positive slope occurs at the centerline and cavitation appears at this higher cavitation number.

Figure 9 shows the specrum of pressure fluctuations p1, p2 and p3 measured with the diffuser and the inlet surge tank, at σ =0.84 The number θ in ( ) shows the phase difference at two different circumferencial locations. The frequency f is normalized with the rotational frequency n of the runner. The amplitude of the pressure fluctuation $\tilde{p}$ is normalized as $\psi = \tilde{p}/(0.5\rho v^2)$ using the runner velocity v at the exit.

We observe a strong surge mode oscillation with $\theta = 0^o$ at overload Q/Q_{ref}=1.17 in p2 near the cavity closure point. No swirl mode oscillations were observed at this higer flow rate. At part load with Q/Q_{ref}=0.5 and 0.33 both surge mode with $\theta = 0^o$ and swirl mode with $\theta = 90^o$ are observed. What is important is that the surge mode frequency is much smaller than the swirl mode frequency, showing that the former is not caused by the latter as generally occurs.

Similar results were obtain without the surge tank, except that the surge mode frequency at part load is somewhat decreased as will be discussed later.

Figure 10 compares the geometries of the cavity between experiment and CFD. At part load of Q/Q_d=0.33, the cavity appears in the corkscrew vortex core. The cavity volume fluctuates with the surge frequency of f/n=0.268 as shown in (a) while rotating at the swirl mode frequency of f/n =1.074, as shown in (b). At higher flow of Q/Q_d=1.17, the experimental result shows the cavity almost fills up the runner discharge. Although a corkscrew vortex structure rotates downstream of the cavity trailing edge, it was not observed as the pressure fluctuation shown in Fig.9. The numerical result at Q/Q_d=1.17 shows that the minimum cavity volume is much smaller than the experimental result. However the cavity almost fills up the runner discharge when the cavity volume is larger.

Figure 11 compares the frequency f normalized with the rotational frequency n under the conditions with and without the surge tank at the runner speed of 3,000rpm and 4,000rpm. CFD results with the boundary conditions of BC1 and BC2 are also shown. At higher flow rate, the surge frequency is not affected by rpm, the existence of the surge tank, and the boundary conditions, showing that it is not caused   and affected by the flow upstream of the runner. However, at part load, the frequency becomes higher with the surge tank or with the boundary condition BC2 allowing the upstream flow rate fluctuation. This can be explained from the resonant frequency
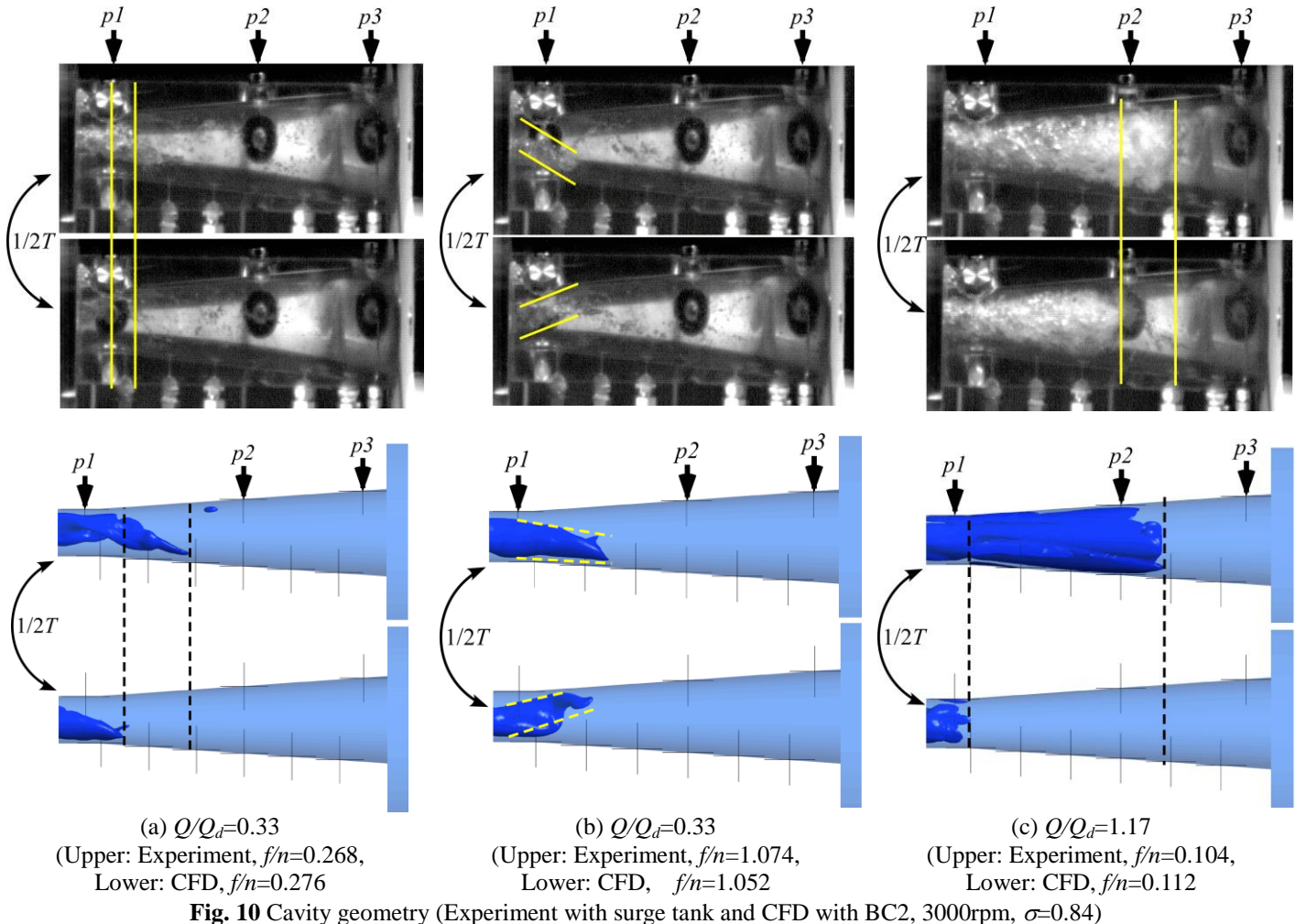
(a) Q/Q_d=0.33
(Upper: Experiment, f/n=0.268,
Lower: CFD, f/n=0.276

(b) Q/Q_d=0.33
(Upper: Experiment, f/n=1.074,
Lower: CFD, f/n=1.052

(c) Q/Q_d=1.17
(Upper: Experiment, f/n=0.104,
Lower: CFD, f/n=0.112

Fig. 10 Cavity geometry (Experiment with surge tank and CFD with BC2, 3000rpm, σ=0.84)

(a) Surge mode
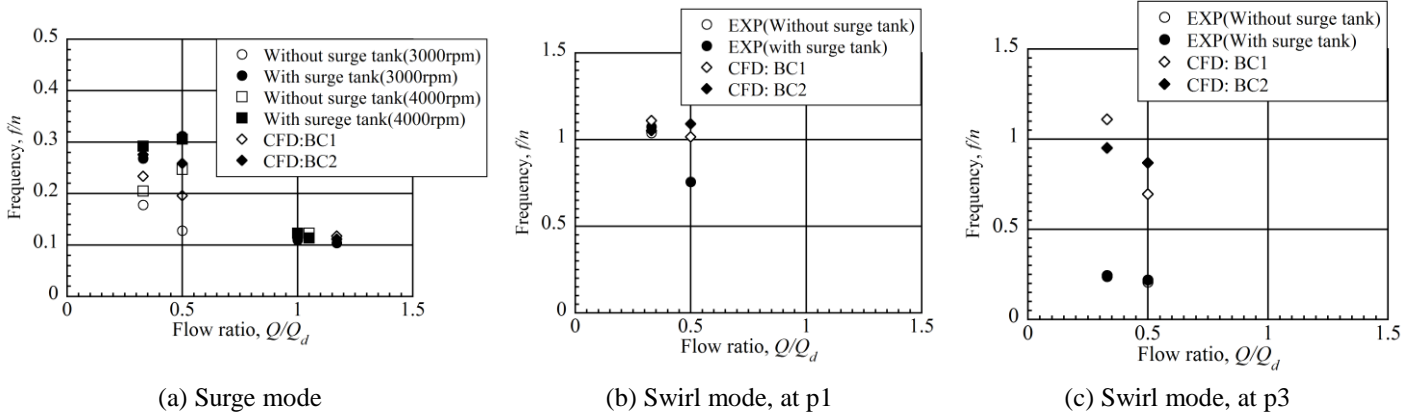
(b) Swirl mode, at p1

(c) Swirl mode, at p3

Fig. 11 Comparison of frequencies with and without surge tank, σ =0.84

$\omega = \sqrt{(M_1 + M_2)K/M_1 M_2}$ of two masses with M_1 and M_2 connected by a spring of rigidity K. When $M_1=M_2$, the frequency becomes $\sqrt{2}$ times of the value with $M_1 \to \infty$.

The swirl mode frequency increases as the decrease of the flow rate, except for the result of CFD assuming constant total pressure at the inlet. The higher swirl mode frequency observed at the location of p3 is caused by 2 cells in CFD and 1 cell in the experiment.

Figure 12 shows the dependence of the surge and swirl mode frequencies on the cavitation number. The surge frequency at higher flow rate is much smaller than that at smaller flow rare. The surge frequency increases with the cavitation number. The swirl mode frequency depends largely on the location where the pressure fluctuation is measured: smaller downstream. This is perhaps caused by the fact that the swirl flow velocity is decreased in the downstream caused by the increase of the diffuser radius, since it was confirmed by CFD that the velocity of vortex whirl is nearly the same as the local flow swirl velocity.

3.2 Cavity volume, upstream and downstream flow rate fluctuations

Figure 13 shows the fluctuations of cavity volume, upstream and downstream flow rate from CFD. We should note first that the flow rate fluctuation occurs such that the continuity equation $dV_C/dt=Q_2-Q_1$ is satisfied. With BC2 and Q/Q_d=0.33, the upstream flow rate
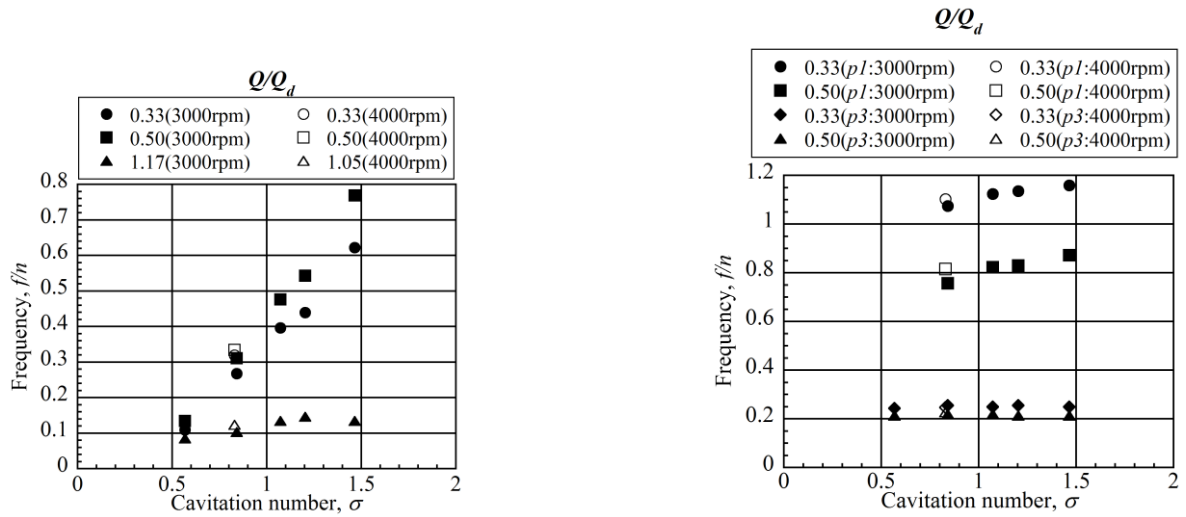
(a) Surge mode   (b) Swirl mode

Fig. 12 Effect of cavitation number on surge and swirl mode frequencies (with surge tank)

(a) CFD:BC1(Q/Q_d=0.33)

(b) CFD:BC1(Q/Q_d=1.17)

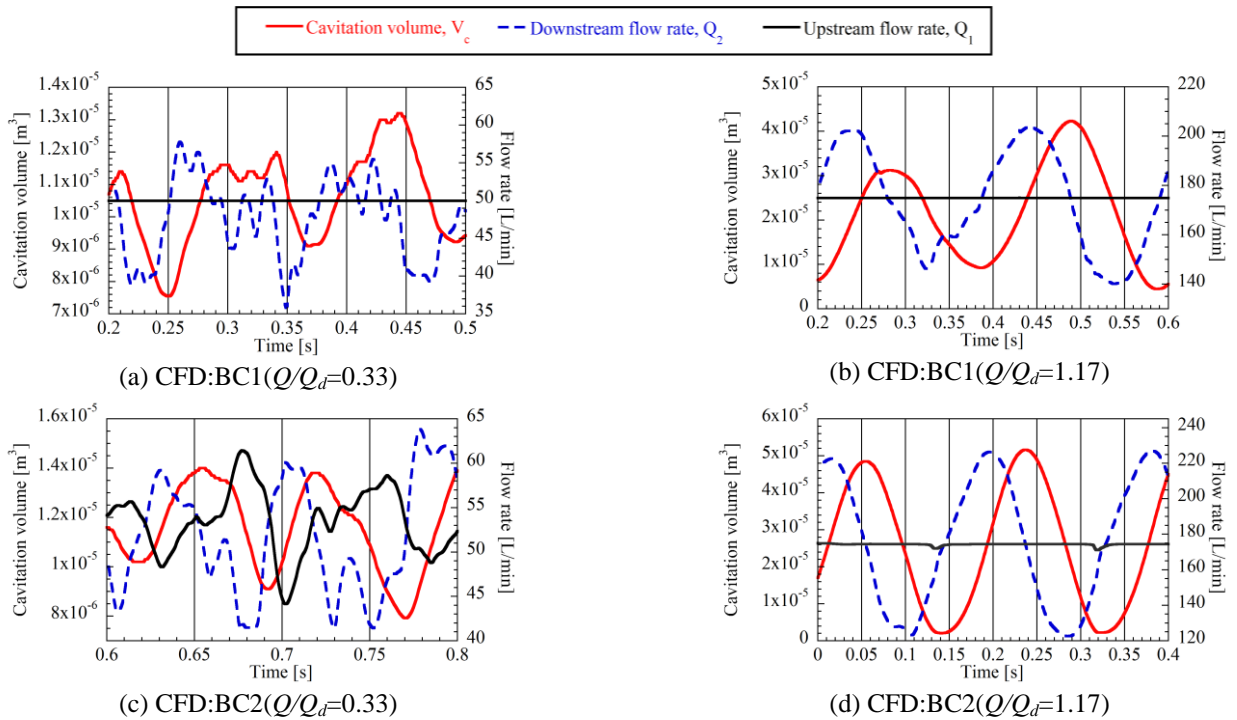(c) CFD:BC2(Q/Q_d=0.33)

(d) CFD:BC2(Q/Q_d=1.17)

Fig. 13 Time-history of flow fluctuation (3000rpm, σ=0.85)

fluctuates with an opposite phase to the downstream flow rate fluctuation. However, at Q/Qd=1.17, the upstream flow flow rate is nearly contant although it is allowed to fluctuate with constant inlet total pressure. This is because the runner exit is fully cavitated as shown in Fig.10(c) and the pressure there is kept nearly constant as shown in Fig.9(a).

As discussed in the introduction, the swirl flow effects destabilize the system when the cavity volume becomes larger when the upstream flow rate is smaller. Fig.13(c) shows that the cavity volume fluctuation occurs with a phase delay of about $\pi/2$ behind this relation. The importance of the phase delay has already been pointed out by Doerfler et al. [7]. The phase delay makes the swirl flow effects at part load to be neutrally stable. The delay can be caused by the time required for the angular momentum to convect from the runner exit to the axial position where the substantial cavity exist. However, Fig.13(c) suggests that it is more plausible that the phase relation between the cavity volume and the flow rate fluctuations occurs simply through the continuity equation.

3.3 Displacement work

In order to study the cause of instabilities, we consider the unsteady displacement work

$$E = \int \tilde{p}d\tilde{V}_c = \int \tilde{p}_i(\tilde{Q}_i dt) - \int \tilde{p}_1(\tilde{Q}_1 dt) = \int \tilde{p}_i d\tilde{V}_i - \int \tilde{p}_1 d\tilde{V}_1 \qquad (2)$$

where tilde means the fluctuating component and $_i$ is a selected location. Discussions are made based on the CFD using BC2. Figure14 and 15 show the plot of p_i against $\tilde{V}_i = \int \tilde{Q}_i dt$. The red curve shows the phase with $d\tilde{V}_i/dt > 0$ and the blue curve $d\tilde{V}_i/dt < 0$.
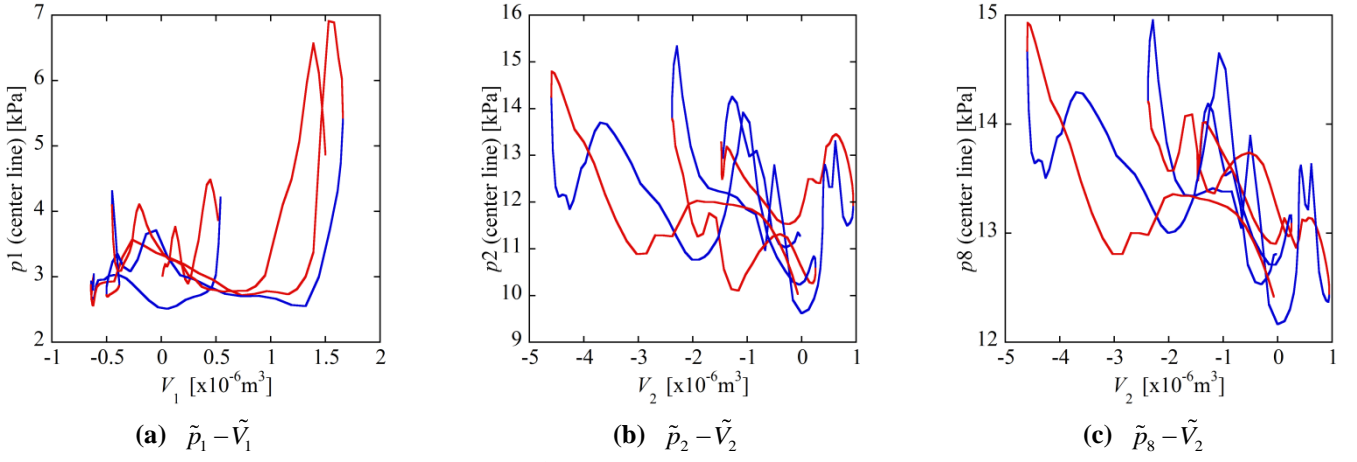
157

(a) $\tilde{p}_1 - \tilde{V}_1$　　　　　　(b) $\tilde{p}_2 - \tilde{V}_2$　　　　　　(c) $\tilde{p}_8 - \tilde{V}_2$

Fig. 14　$\tilde{p}_i - \tilde{V}_i$　plot at Q/Q_d=0.33　(CFD　with　BC2)

(a) $\tilde{p}_1 - \tilde{V}_1$　　　　　　(b) $\tilde{p}_2 - \tilde{V}_2$　　　　　　(c) $\tilde{p}_8 - \tilde{V}_2$
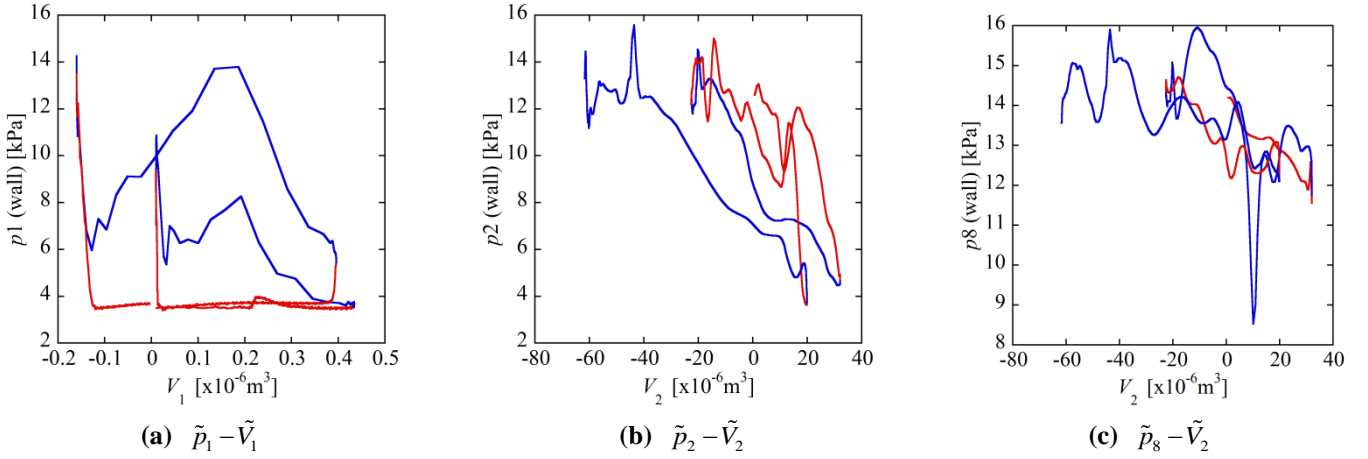
Fig. 15　$\tilde{p}_i - \tilde{V}_i$　plot at Q/Q_d=1.17　(CFD　with　BC2)

Clockwise Lissajous means positive work transfer from upstream to downstream. Wall pressure is used for Q/Q_d=1.17 since the central part is occupied by cavity and the pressure at the center is used for Q/Q_d=0.33 since the wall pressure does not show the pressure recovery as shown in Fig.8.

The $\tilde{p}_1 - \tilde{V}_1$ plots show streamwise work transfer at Q/Q_d=0.33 while anti-streamwise work transfer occurs Q/Q_d =1.17 although the amplitude of $\tilde{V}_1$ is very small for Q/Q_d =1.17. At low flow rate of Q/Q_d=0.33, both $\tilde{p}_2 - \tilde{V}_2$ and $\tilde{p}_8 - \tilde{V}_2$ plots show that the energy is transferred upstream from the diffuser to the cavity. This can be explained from the unsteady Bernoulli equation for non-swirl flow.

$$p_2 - p_{exit} = \rho \frac{L_e}{A_e} \frac{dQ_2}{dt} + \rho \frac{\zeta - D}{2A_e^2} Q_2^2 \qquad (3)$$

where, $L_e = \int A_e / A(s)ds$ is the inertance and $D = (A_e / A_2)^2 - 1 > 0$ is the diffusion factor (Ae is the diffuser exit area) and is assumed to be larger than the loss coefficient ζ, suggesting larger pressure recovery (smaller p_2) with larger Q_2. This was also found in non-swirl flow[4]. However, the $\tilde{p}_2 - \tilde{V}_2$ plot at Q/Q_d =1.17 shows reversed energy transfer. This may be caused by the wake of cavity which extends to p2 location.

3.4 Cause of cavitation surge

The above observations suggest that the draft tube surge is caused by the diffuser effect of the draft tube.   To confirm this, tests were carried out by attaching an orifice at the diffuser outlet. The orifice has an aperture with the same diameter as the diffuser inlet so that the "diffuser effect" is completely cancelled. Figure 16 compares the spectrum of the pressure fluctuation with and without the orifice. The comparisons were made at different cavitation number but at similar cavity size near the runner exit, although the cavity extends to the orifice at Q/Q_d=0.33. The amplitude of the pressure fluctuation is significantly decreased with the orifice. However, at Q/Q_d=0.33, we still have a spectrum peak, suggesting that there can be some cause of the instability other than the diffuser effects.

Experiments were carried out also with a straight pipe in place of the diffuser and the results are shown in Fig.17. The over load surge at Q/Q_d=1.17 does not occur. However, at part loads, we observe the surge mode with similar frequency as with the diffuser. The swirl mode component is found near the exit.
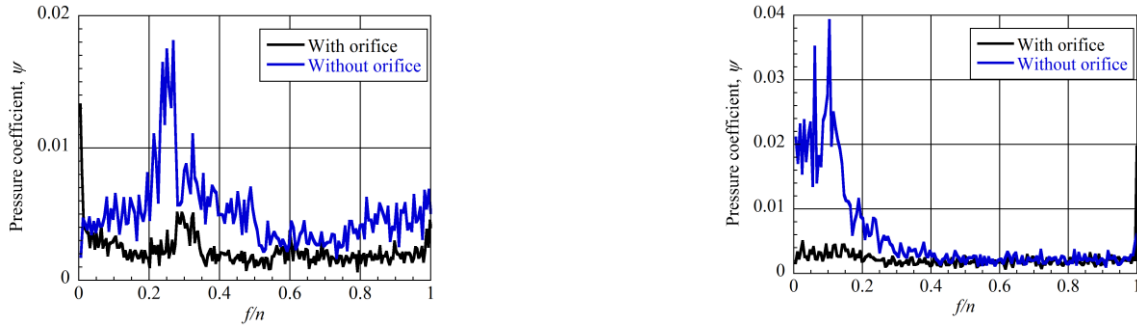
(a) Q/Q_d=0.33, z/d_i=3.0($p2$), $\sigma = 0.83$ without orifice, $\sigma = 0.18$ with orifice.

(b) Q/Q_d=1.14, z/d_i=-0.32($p1$), $\sigma = 0.29$ without orifice, $\sigma = 1.42$ with orifice.

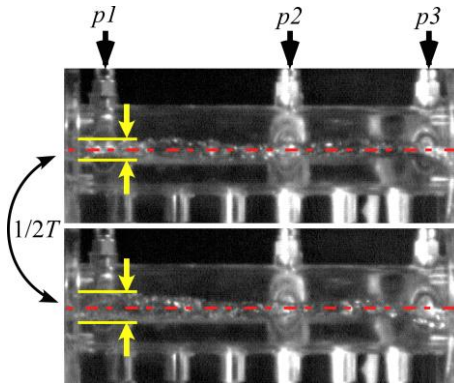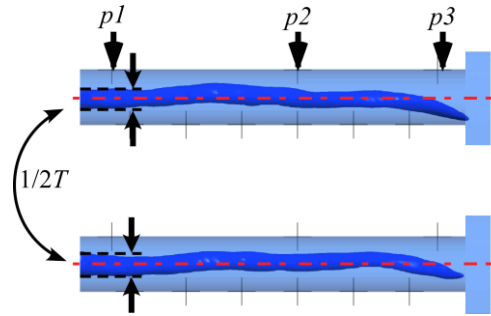**Fig. 16** Pressure fluctuation with and without orifice, with surge tank
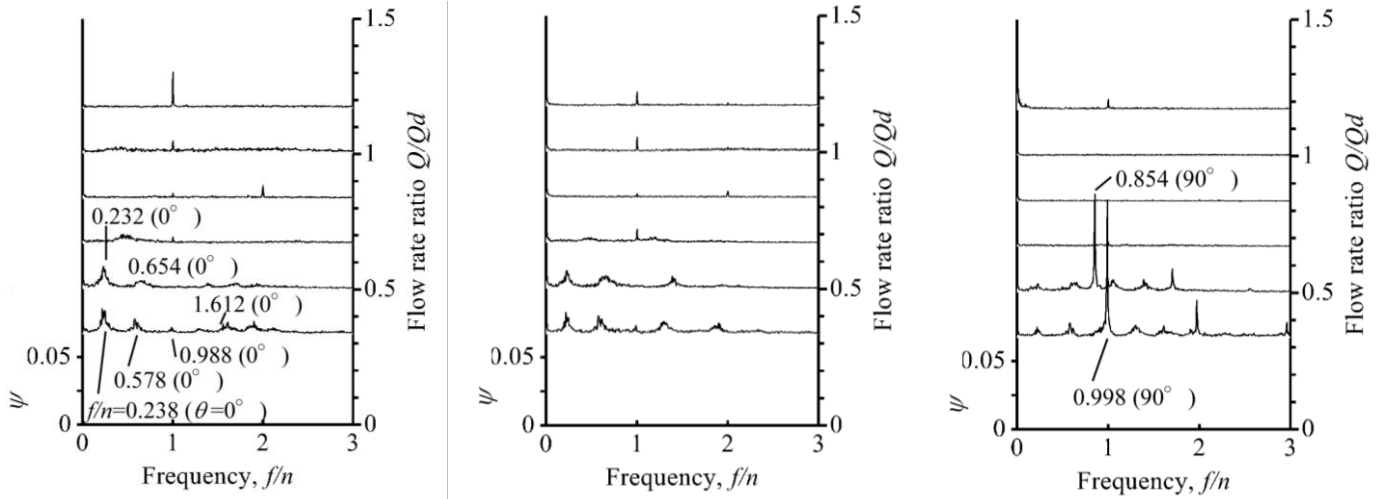
(a) $p1$　　　　　　　　　(b) $p2$　　　　　　　　　(c) $p3$

Fig. 17 Pressure spectrum with straight pipe, with surge tank (3000rpm, σ =0.86)

(a) Experiment(Without surge tank)
(Time interval=0.056sec, f/n=0.148)

(b) CFD:BC1 (Iso-surface of void fraction = 0.01, Time interval =0.055sec, f/n=0.182)

Fig. 18 Comparison of unsteady behavior of cavitation between experiment and CFD (Surge mode, σ =0.87, Q/Q_d=0.33)

Figure 18 compares the cavity geometry between experiment and CFD. The cavity extends to the exit and the whirl occurs near the exit. It was found by the examination of the phase at different axial locations that the disturbance is propagating from the exit to upstream. This type of oscillation was found also in a test with a swirler [3].

4. Conclusion

It was shown that surge occurs both at higher and lower flow rates than the swirl free flow rate, both with and without a surge tank at the volute inlet. At higher flow, the cavity appears mainly at the center of the runner exit while it occurs in the center of corkscrew vortex at smaller flow rates. The frequency of higher flow surge is not affected significantly by the existence of the surge tank, while the frequency of lower flow surge was higher with a surge tank. The swirl mode pressure fluctuation was observed only at part load and the frequency was much larger than the surge mode frequency. So, the surge mode at smaller flow rate observed in the present study is not caused by the precession of spiral vortex rope. The above character was simulated by CFD using the boundary condition of constant flow rate at the volute inlet for the case without the surge tank, and with the boundary condition of constant total

pressure for the case with the surge tank. With the CFD, the upstream flow rate fluctuation occurs at lower flow rate with its phase relative to the cavity volume fluctuation such that the continuity equation is satisfied. However, the upstream flow rate fluctuation did not occur even with the boundary condition of constant total pressure, because the runner exit pressure was kept nearly constant with the cavity.

The above observations show that the surge is caused by a flow mechanism in the downstream. To examine if it is attributed to the diffuser effects, additional tests with an orifice at the diffuser exit and with the diffuser replaced with a straight pipe were carried out. The surge at higher flow disappeared with these arrangements. So, the higher flow surge can be concluded to be caused by the diffuser effects. Although the amplitude of the small flow surge was significantly decreased with the orifice, a surge mode with similar frequency appeared with the straight pipe. The surge mode observed with the straight pipe was such one that the disturbance is propagating from the pipe exit to the runner. Although this might be different from that observed with a diffuser, further study is needed to clarify the cause of the surge at part load.

Acknowledgments

Nomenclature

f : Pressure fluctuation frequency [Hz]

n : Runner rotational frequency [Hz]

p_T : Gas phase pressure in tank [Pa]

p_v : Vapor pressure [Pa]

p : Pressure [Pa]

Q : Flow rate [L/min]

Q_d : Design flow rate [L/min]

ρ : Density [kg/m^3]

σ : Cavitation number

T : Period of pressure fluctuation, $1/f$ [s]

ψ : Pressure coefficient

z : Axial coordinate [m]

References

[1] Chen, C., Nicolet, C., Yonezawa, K., Farhat, M., Avellan F., and Tsujimoto, Y., 2008, "One-Dimensional Analysis of Full Load Draft Tube Surge", Journal of Fluids Engineering, 130, Issue 4.

[2] Chen, C., Nicolet, C., Yonezawa, K., Farhat, M., Avellan F., and Tsujimoto, Y., 2009, "One-Dimensional Analysis of Full Load Draft Tube Surge Considering the Finite Sound Velocity in the Penstock", International Journal of Fluid Machinery and Systems, 2, No. 3, 260-268.

[3] Chen, C., Nicolet, C., Yonezawa, K., Farhat, M., Avellan F., and Tsujimoto, Y., 2010, "Experimental Study and Numerical Simulation of Cavity Oscillation in a Diffuser with Swirling Flow", International Journal of Fluid Machinery and Systems, Vol. 3, No. 1, 80-90.

[4] Chen, C., Nicolet, C., Yonezawa, K., Farhat, M., Avellan F., and Tsujimoto, Y., 2010, "Experimental Study and Numerical Simulation of Cavity Oscillation in a Conical Diffuser", International Journal of Fluid Machinery and Systems, 3, No. 1, 91-101.

[5] Nishi, M., Surging Characteristics of Conical and Elbow Type Draft Tubes, Proc. 12th IAHR Symposium on Hydraulic Machinery and System, Stirling (1984), 272-283.

[6] Doerfler, P. K., Francis Turbine Surge Prediction and Prevention, Proc. Waterpower ' 85(1985), 952-961.

[7] Doerfler, P.K., Keller, M., and Braun, O., 2010, "Francis full-load surge mechanism identified by unsteady 2-phase CFD," IAHR 25th Symp. On Hydr. Mach. Systems, Timisoara, 2010.